Photochemical & Photobiological Sciences

Dynamic Article Links

Cite this: *Photochem. Photobiol. Sci.*, 2012, **11**, 1210

www.rsc.org/pps

PAPER

Sequential photoisomerisation dynamics of the push–pull azobenzene Disperse Red 1

Julia Bahrenburg, Katharina Röttger, Ron Siewertsen, Falk Renth* and Friedrich Temps*

Received 8th December 2011, Accepted 22nd March 2012
DOI: 10.1039/c2pp05400k

The ultrafast dynamics of the push–pull azobenzene Disperse Red 1 following photoexcitation at λ_{pump} = 475 nm in solution in 2-fluorotoluene have been probed by broadband transient absorption spectroscopy and fluorescence up-conversion spectroscopy. The measured two-dimensional spectro-temporal absorption map features a remarkable "fast" excited-state absorption (ESA) band at $\lambda \approx 570$ nm appearing directly with the excitation laser pulse and showing a sub-100 fs lifetime with a rapid spectral blue-shift. Moreover, its ultrafast decay is paralleled by rising distinctive ESA at other wavelengths. Global fits to the absorption–time profiles using a consecutive kinetic model yielded three time constants, $\tau_1 = 0.08 \pm 0.03$ ps, $\tau_2 = 0.99 \pm 0.02$ ps, and $\tau_3 = 6.0 \pm 0.1$ ps. Fluorescence–time profiles were biexponential with time constants $\tau_1' = 0.12 \pm 0.06$ ps and $\tau_2' = 0.70 \pm 0.10$ ps, close to the absorption results. Based on the temporal evolution of the transient spectra, especially the "fast" excited-state absorption band at $\lambda \approx 570$ nm, and on the global kinetic analysis of the time profiles, τ_1 is assigned to an ultrafast transformation of the optically excited ππ* state to an intermediate state, which may be the nπ* state, τ_2 to the subsequent isomerisation and radiationless deactivation time to the S_0 electronic ground state, and τ_3 to the eventual vibrational cooling of the internally "hot" S_0 molecules.

1. Introduction

The reversible $E \rightleftarrows Z$ photoisomerisation reaction of azobenzene (AB) forms the basis for numerous applications of AB derivatives as photochromic molecular switches, tiny light-driven molecular manipulators, actuators and engines, or smallest optical memory and logical devices.[1–6] The high potential of AB as photoswitchable element rests on the large changes in molecular size, shape and dipole moment induced by light at ultraviolet to visible (UV/VIS) wavelengths and on the low photochemical fatigue of the chromophore. To reach many ambitious rational design goals for optimised functional AB devices, however, it is mandatory to have detailed knowledge about the ensuing molecular dynamics under different circumstances.

Of major importance for applications is that substituents at the AB core may hugely affect the photoisomerization dynamics by electronic and by steric effects. A special class are electron donor–electron acceptor substituted AB dyes like Disperse Red 1 4-[*N*-ethyl-*N*-(2-hydroxyethyl)amino]-4′-nitro-azobenzene, DR1; Scheme 1].

DR1 is a so-called push–pull azobenzene, in which the donor–acceptor substitution introduces a strong charge transfer (CT) character into the ππ* electronic transition.[4,7,8] Compared to unsubstituted AB, this leads to a large red-shift of the ππ* absorption band from the near-UV into the visible spectrum such that it overlaps with the normally much weaker nπ* transition.[9–11] At the same time, the energy barrier between the two isomers in the S_0 electronic ground state is lowered to the extent that the thermal $Z \rightarrow E$ back-isomerisation at room temperature happens in times of just seconds to milliseconds, depending on the solvent, much faster than in normal AB.[12,13] These factors, together with the large photo-induced structural change, determine the specific application profile for, *e.g.*, tailored surface functionalisation, light-induced material deformation, surface-relief formation, nonlinear optics, or charge separation in organic photovoltaic and ferroelectric materials.[7,14–19] DR1 is of particular practical interest because of its hydroxy group, which can be employed as a covalent linker, for example by functionalizing it with a methacrylate group for embedding in a polybutylmethacrylate (PBMA) matrix.[20]

In contrast to plain AB, where the photoisomerisation mechanism is well studied,[21–31] the molecular dynamics of DR1 and related push–pull substituted ABs following excitation in the strong visible ππ*-type absorption band still remains controversial, despite several spectroscopic[32,33] and time-resolved[10,11,34,35]

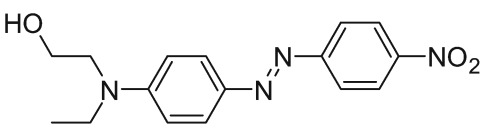

Disperse Red 1 (DR1)

Scheme 1

Institut für Physikalische Chemie, Christian-Albrechts-Universität zu Kiel, Olshausenstr. 40, D-24098 Kiel, Germany.
E-mail: renth@phc.uni-kiel.de, temps@phc.uni-kiel.de

experimental studies and theoretical calculations.[11,36–39] This includes the question of the energetic ordering of the first nπ* and ππ* electronic states of the molecules and their distinctive roles in the photoisomerisation and electronic deactivation processes.[10,11,36,37] It is undoubted at present only that both electronic states are very close. Radiationless interconversion between them should therefore be feasible and fast.

For the case of 4-methoxy-4′-nitro-azobenzene (MNAB), which has been measured by femtosecond transient absorption spectroscopy by Hagiri *et al.*,[9] the $S_1(n\pi^*) < S_2(\pi\pi^*)$ energetic order of states seems established. However, it is not clear whether this also holds for DR1, since methoxy is a much weaker electron donor than a dialkylamino group. A time-resolved fluorescence and absorption study of 4-dimethylamino-4′-nitro-azobenzene (DMANAB) by Schmidt *et al.* revealed a bi-exponential decay behavior with time constants of $\tau_1 \approx 100$ fs and $\tau_2 \approx 1$ ps.[10] As τ_1 was associated with a rapid departure of the wavepacket from the Franck–Condon (FC) region of the photo-excited ππ* state and τ_2 with the isomerisation and electronic deactivation to the S_0 state, the photo-induced dynamics was concluded to be analogous to plain AB.[10] A later paper on the ultrafast kinetics and anisotropy of the excited-state absorption of DR1 in different solvents by Poprawa-Smoluch *et al.* assumed that the nπ* state was reached from the initially excited ππ* state,[11] but the experimental time resolution was insufficient to fully resolve the dynamics of both states. More recently, Hsu *et al.* investigated the similar push–pull AB Disperse Red 19 and observed time constants of $\tau_1 = 0.10$ ps and $\tau_2 = 1.11$ ps,[35] which they interpreted in the same way as Schmidt *et al.*[10] for DMANAB, without much further discussion of the nature or possible sequential dynamics of the involved states. Quantum chemical calculations on the photo-induced reaction routes reported for several push–pull substituted ABs,[38,39] including DR1,[11,36,37] favour the rotational isomerisation mechanism as in plain AB.[22,25,26,28,31]

Static spectra of DR1 and related push–pull ABs in solution and the quantum chemical calculations generally suggest that the ππ* state is higher in energy than the nπ* state, unless the solute and solvent form strong H-bonds.[11,36,37] The virtual absence of fluorescence from DR1 in aprotic solvents from *n*-hexane to acetonitrile has been explained by fast internal conversion from the excited ππ* to the nπ* state, which has almost no oscillator strength to the S_0 state. Fluorescence spectra and quantum yields, excitation spectra, and excitation anisotropies of DR1 in a series of alcohols as examples for polar, protic and H-bonding solvents reveal that the nπ* and ππ* states have almost the same adiabatic excitation energies, but that the ππ* state is reached first upon vertical excitation.[36] However, the picture becomes considerably more complex if one tries to distinguish between the ππ*-type local optically excited (OE) state and an energetically lower "relaxed" CT state supposed to be formed from the OE state. A resonance Raman study on the solvent influence and the contributions of solvent relaxation and reorganisation on the molecular structure and ultrafast isomerisation dynamics of DMANAB by Biswas and Umapathy showed that the polarity of the solvent plays a decisive role for the excited-state structure and energy and confirmed the strong CT character in the optical transition,[32,33] but a clear and unambiguous picture still remains to be developed.

This paper reports on a study of the photo-induced ultrafast dynamics of DR1 by femtosecond time-resolved broadband absorption spectroscopy and fluorescence up-conversion following excitation at $\lambda_{pump} = 475$ nm. Special attention is directed at the observation of an ultrafast transient excited-state absorption band between $\lambda_{probe} \approx 530$–580 nm rising immediately with the excitation laser pulse, earlier than slightly delayed transient excited-state absorptions at other detection wavelengths. This feature provides strong support for a stepwise electronic deactivation and isomerisation mechanism from the ππ* optically excited state (OE) to the S_0 ground state *via* an intermediate excited (IE) state. The recorded absorption–time profiles in the range from $\lambda_{probe} = 350$–680 nm are therefore analysed in a consistent fashion using a sequential kinetic model and global fitting. The supposed IE state is discussed in the light of the time-resolved results and the evidence from static absorption and fluorescence[36,37] and resonance Raman spectra.[32,33]

2. Experimental section

All time-resolved measurements in the present work were performed at room temperature in flow cells of 1 mm optical path length with 0.2 mm quartz windows. The samples of Disperse Red 1 (>96%) and the solvent 2-fluorotoluene (2FT, >96%) were used as supplied (Sigma-Aldrich). Solutions at concentrations of 0.03 mM corresponding to an optical density of ≈0.5 at the excitation wavelength were pumped through the probe cells with a peristaltic pump (Ismatec). The solvent 2FT was employed in the present work because it is nearly isorefractive with PBMA, which allows for highly sensitive femtosecond photodynamics measurements on DR1-functionalised PBMA-nanopolymers. These results will be reported elsewhere.[20]

2.1. Broadband transient absorption measurements

The experimental setup for femtosecond time-resolved broadband absorption spectroscopy in our laboratory is based on a regeneratively amplified Ti:Sa laser (Clark MXR CPA2001).[40,41] Pump pulses at $\lambda = 475$ nm with typically ≈0.5 μJ per pulse and ≈35 fs duration (Gaussian fwhm) were delivered by a home-built non-collinear optical parametric amplifier (NOPA). Supercontinuum probe and reference pulses between 350 nm ≤ λ_{probe} ≤ 700 nm were generated in CaF_2. The pulses were focused into the sample cell at an angle between pump and probe of 5°. The transmitted probe and reference spectra were taken using an imaging spectrograph with a 1024 × 127 pixel CCD camera. A BG18 filter before the spectrograph attenuated the intense near-IR part of the supercontinuum. The pump–probe time delay was set using a computer-controlled translation stage.

The pump-induced cross-phase modulation (XPM) and stimulated Raman scattering (SRS) signals were measured independently for the pure solvent. Two-dimensional transient absorption maps were then obtained by subtracting the XPM and SRS contributions from the sample spectra taking into account the pump pulse absorption by the sample and the time-zero correction for each wavelength determined from the XPM signal. The width of the instrument response function (IRF) estimated from the SRS signal was about 110 fs (fwhm), which allows for

a time resolution of the experiment of $\Delta t \approx 30$–40 fs. The shape of the observed XPM signal around time-zero was taken as input for the non-linear least-squares fitting analysis of the absorption–time profiles.

2.2. Fluorescence up-conversion measurements

Time-resolved fluorescence measurements were performed using the up-conversion technique.[42,43] The emission by the sample molecules excited by a second NOPA (0.3 μJ per pulse) was collected and focused into a BBO crystal for up-conversion by type II sum frequency generation with the 775 nm Ti:Sa gate pulses by a pair of off-axis parabolic mirrors. The up-converted light passed a double monochromator and was detected as function of the pump-gate delay time by a photomultiplier connected to a gated photon counter. An OG550 band pass filter was placed behind the sample cell to remove scattered pump photons. Pump-gate cross correlation determined an IRF width of ≈200 fs (fwhm), corresponding to a time resolution of $\Delta t \approx 80$ fs.

3. Results

3.1. Stationary spectra

The stationary UV/VIS absorption and fluorescence spectra of DR1 in 2FT are displayed in Fig. 1. Also plotted are the absorption spectra of DR1 in the nonpolar solvent *n*-hexane and in the polar protic ethanol and the absorption spectrum of unsubstituted AB in *n*-hexane for comparison. As shown, the strong ππ*-type absorption band of DR1 has its maximum at $\lambda = 445$ nm in *n*-hexane (dielectric constant $\varepsilon = 1.9$), $\lambda = 475$ nm in 2FT ($\varepsilon = 4.2$) and $\lambda = 482$ nm ethanol ($\varepsilon = 24$),[44] respectively. The CT character of the excited state is reflected by the large solvatochromic red-shift with increasing solvent polarity.[8,11,37] Accordingly, 2FT is ranked as a relatively polar medium. The much weaker nπ* transition, observed in plain AB at $\lambda = 450$ nm, remains hidden under the intense ππ* band. It should be less affected by the push–pull substitution and the polarity of the solvent.[11,36]

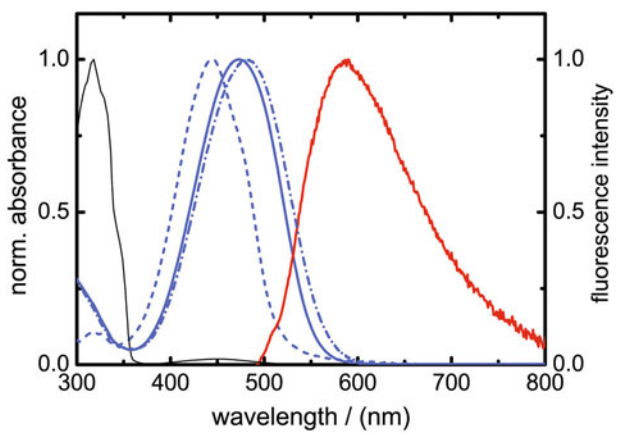

Fig. 1 Normalised stationary absorption spectrum of DR1 in *n*-hexane (dashed blue), 2FT (solid blue) and ethanol (dash-dotted blue) and stationary fluorescence spectrum of DR1 in 2FT (solid red). The absorption spectrum of plain AB in *n*-hexane is shown by the thin black line for comparison.

The fluorescence spectrum of DR1 excited at $\lambda = 475$ nm shows a broad asymmetric emission band between 500 nm $\leq \lambda_{fl} \leq$ 800 nm with its maximum in 2FT at $\lambda_{fl} \approx 590$ nm. The pronounced Stokes shift by ≈115 nm with respect to the absorption maximum underlines the CT character of the excited state, which experiences significant stabilisation by a polar solvent. The time-resolved measurements in the following will shed more light on the involved excited states.

3.2. Transient absorption measurements

Fig. 2 displays the two-dimensional spectro-temporal map of the change in optical density ΔOD after photoexcitation of the DR1 sample in 2FT at $\lambda_{pump} = 475$ nm for delay times up to $\Delta t = 10$ ps. The pump wavelength coincides with the peak of the ππ* absorption band of the molecules. The dynamics were followed up to $\Delta t_{max} = 65$ ps, but only little change was observed beyond $\Delta t = 10$ ps. The detection wavelengths range from $\lambda_{probe} = 350$–680 nm.

The spectro-temporal data map (Fig. 2) shows an intensive bleach of the absorption around $\lambda = 475$ nm immediately after the pump pulse at $\Delta t = 0$. This so-called ground state bleach (GSB) extends between 420 nm $\leq \lambda_{probe} \leq 525$ nm. At the same time, several excited-state absorption (ESA) bands appear. At least three distinctive spectral regions can be distinguished, from $\lambda_{probe} = 350$–415 nm, 530–580 nm, and ≈580–670 nm. All ESA bands decay almost completely within the first one to two picoseconds. The somewhat longer-lived signal around 530–580 nm is attributed to absorption by vibrationally hot ground state molecules (HGSA) resulting from the electronic deactivation. The ensuing processes lead to a recovery of most of the GSB, but a significant permanent GSB remains at the longest experimental delay time ($\Delta t_{max} = 65$ ps), where all electronic and vibrational

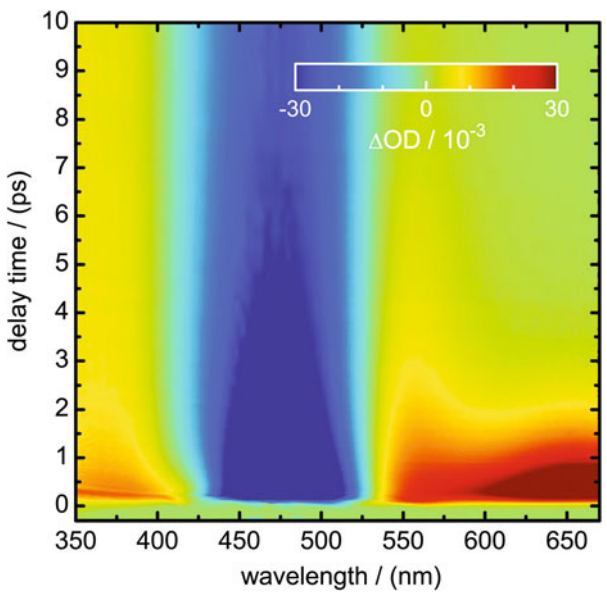

Fig. 2 Two-dimensional map of the change in optical density (ΔOD) following excitation of the DR1 sample molecules at $\lambda_{pump} = 475$ nm for probe wavelengths in the range 350 nm $\leq \lambda_{probe} \leq 680$ nm and delay times of $\Delta t \leq 10$ ps. Little change was observed at $\Delta t > 10$ ps up to the maximum experimental delay time of 65 ps.

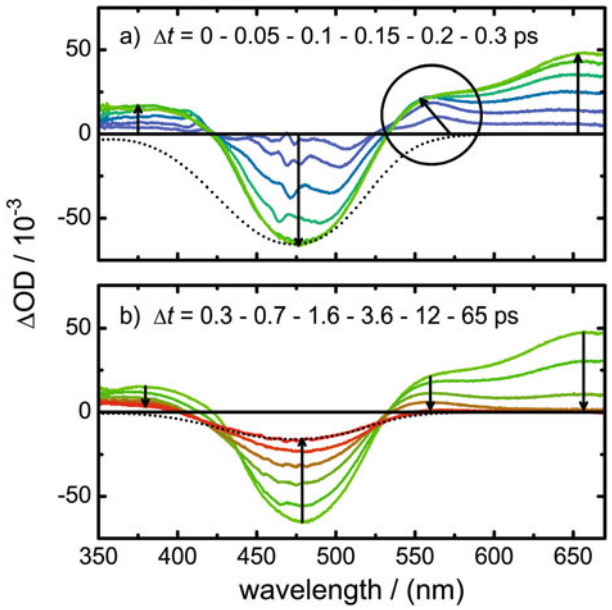

Fig. 3 Transient spectra of DR1 at different delay times between $0 \leq \Delta t \leq 0.3$ ps (blue to green, top) and between 0.3 ps $\leq \Delta t \leq 65$ ps (green to red, bottom) after the pump pulse at $\lambda = 475$ nm. The arrows indicate the temporal evolution of the transient spectra. The circle in the upper panel showcases the rise and blue-shift of the "fast" ESA band from $\lambda_{probe} \approx 570$ to $\approx$550 nm. The black dashed lines show the (negative) absorption of DR1 scaled to the peak GSB (upper panel) and the final absorption at $\Delta t = 65$ ps (lower panel).

relaxation processes are over. This final GSB signal thus reflects the $E \rightarrow Z$ isomerisation reaction of the DR1 molecules. The formation of *Z*-DR1 is witnessed by the permanent positive product absorption (PA) band between $\lambda_{probe} = 350$–400 nm that can be seen to remain constant at the longest delay times.

The transient spectra at selected delay times displayed in Fig. 3 reveal the ensuing photo-induced molecular dynamics in some more detail. The upper panel (Fig. 3a) shows the ultrafast spectro-temporal evolution within the first 300 fs after the excitation laser pulse, the subsequent changes up to $\Delta t_{max} = 65$ ps are given in the lower panel (Fig. 3b). The characteristic GSB and ESA bands (as well as HGSA and PA at later delay times) are nicely featured in the distinctive spectral windows identified above. The main changes occur within the first 300 fs and in the next $\approx$1.5 ps thereafter.

The most remarkable feature is the ultrafast, instrument-limited rise of ESA at wavelengths from 530–580 nm (ESA_1, for reference below) that is clearly faster than the rise of the ESA features appearing with some delay at $\lambda \approx 580$–670 nm (ESA_2) and 350–415 nm (ESA_3). This is clearly evident from the transient spectra in Fig. 3a, where ESA_1 has already reached its maximum at an experimental delay time of no more than $\Delta t \approx$ 125 fs, extremely rapidly, while ESA_2 (and ESA_3) at the same delay time are still at $\lesssim$50% of their eventual maxima. As can be seen, ESA_2 (and ESA_3) need at least $\Delta t \approx 300$ fs to reach their maximal values. Moreover, ESA_1 exhibits a significant spectral blue-shift in the first $\approx$125 fs. ESA_1 is visible despite the fact that its effective peak intensity may be diminished by some overlap with the neighboring negative GSB band and by possible stimulated emission (SE) that might be hidden underneath the excited-state absorption in the spectral window (*cf.* Fig. 1). As will be argued below, the ultrafast rise of ESA_1 from 530–580 nm and its clearly shorter lifetime compared to ESA_2 at >580 nm strongly suggest a sequential, step-wise isomerisation and electronic deactivation mechanism.

The prompt appearance of the very short-lived ESA_1 band with the excitation pulse without delay has not been given full attention before, presumably because its subsequent decay is partially masked by the blue wing of the rising ESA_2 band and by HGSA appearing at slightly longer times ($\Delta t \gtrsim 1$ ps). The delayed appearance of ESA_2 (and ESA_3), on the other hand, has been noted previously.[10,11] Both observations will be accounted for by the analysis of the absorption–time profiles below.

The second important observation is the permanent final absorption at $\lambda < 400$ nm by the photochemically produced *Z*-DR1 isomer. As can be seen from the stationary absorption spectrum in Fig. 1 and from the spectrum at $\Delta t = 0$ in Fig. 3a, there is little absorption by the *E*-form of DR1 at those wavelengths. Judged from the ratio of the final GSB to the GSB at $\Delta t = 0$ for $\lambda_{probe} = 475$ nm, the photoisomerisation quantum yield of DR1 is $\Phi_{E \rightarrow Z} < 0.25$. The upper limit would apply, if the absorbance by the *Z*-DR1 product at $\lambda \approx 475$ nm was practically negligible compared to the initial *E*-DR1.

The temporal development of the transient absorption features is reflected by the absorption–time profiles for four selected probe wavelengths representing the four distinctive spectral windows depicted in Fig. 4. Also shown are the best-fit curves to the data from a global nonlinear least-squares analysis assuming a consecutive kinetic scheme of the type

$$E \xrightarrow{+h\nu} E^* \xrightarrow{\tau_1} E^{**} \xrightarrow{\tau_2} [E^{\#} + Z^{\#}] \xrightarrow{\tau_3} [E + Z]$$

where E^* and E^{**} represent the excited molecules in two different "states" which give rise to the prompt and the delayed ESA, respectively, $E^{\#}$ and $Z^{\#}$ denote vibrationally hot S_0 state molecules responsible for HGSA, and *E*, *Z* denote the final products in their *E*- and *Z*-isomeric forms. The distinction between E^* and E^{**} and the proposition that E^{**} develops consecutively from E^* are made guided by the evidence from the transient spectra (Fig. 3a) and the earlier reports of a delayed ESA rise,[10,11] although the question of the nature of those states has to be deferred to the Discussion below. The time profiles included in the global fit are distributed across the probe wavelength range with an emphasis on the "kinetically cleaner" spectral windows, from which the molecular time constants could be well determined. The time-zero and the IRF width, taken into account by convolution, were kept fixed for all time profiles at the values determined by the XPM and SRS signals to exclude correlation and cancellation effects with time constant τ_1.

The best-fit results for the time constants τ_1–τ_3 in the above kinetic scheme are compiled in Table 1. The most important spectral windows with respect to the excited-state dynamics are those from $\lambda_{probe} = 580$–670 nm and 530–580 nm. As can be seen from the transient absorption data and the fit for $\lambda_{probe} =$ 650 nm in Fig. 4d as an example, τ_2 determines the observed single-exponential ESA_2 decay in the first window. The rise of ESA_2 was described by τ_1 to account for the delayed appearance. Here, both ESA_1 and ESA_2 are important at $\lambda_{probe} =$ 530–580 nm (see Fig. 4c), where τ_1 is well determined by the

decay of ESA_1 *and* the rise of ESA_2 at the earliest times (Fig. 4c left). The distinctive contribution by HGSA in the same wavelength window at later times (Fig. 4c right) is well described by τ_2 for its rise and τ_3 for its slower decay. Continuing towards shorter probe wavelengths, all three time constants (τ_1, τ_2, τ_3) determine the transients at λ_{probe} = 450 nm (Fig. 4b) and λ_{probe} = 360 nm (Fig. 4a), but essentially only their amplitudes remain adjustable. The permanent GSB at 450 nm (Fig. 4b) is accounted for by a step function with IRF-limited rise time. The resulting final values for the three time constants are

$$\tau_1 = 0.08 \pm 0.03 \text{ ps},$$

$$\tau_2 = 0.99 \pm 0.02 \text{ ps},$$

$$\tau_3 = 6.00 \pm 0.10 \text{ ps}.$$

The quoted error limits include the 2σ statistical uncertainty limits and estimated systematical errors, which may result mostly from the error in the IRF width (τ_{IRF} = 0.06 ± 0.01 ps) and the uncertainty in the time-zero value (≈±0.010 ps).

Compared with simpler fit models with only one ESA component (and no delayed rise), the consecutive kinetic scheme yielded a much smaller standard deviation (by a factor of 2.5) of the global fit to all twelve data curves. Additionally, we note that the measured time profiles in the 530–580 nm window could not be modeled well in shape at all assuming only a single ESA decay component. The derived values for τ_1–τ_3 have low correlation and hold within their respective error limits although the applied fit model comprises quite a number of adjustable parameters, because each τ_i usually governs a time profile in a specific wavelength window. The value for τ_2, for example, is in practice fully determined by the three absorption–time profiles taken between λ = 600–650 nm (see Table 1), where this is the only relevant time parameter. With τ_2 thereby controlled, the values for τ_1 and τ_3 are essentially determined by the four data curves in the λ = 575–560 nm window at short and at long delay times, respectively. The absorption profiles at shorter wavelengths (λ = 475–350 nm) are more complex, because they consist of ESA, HGSA, GSB and PA components, but the global fit allows for little variation of the values for τ_1–τ_3 without compromising the fits at the above wavelengths. As a final additional check, we performed an independent global analysis of the full 2D spectro-temporal absorption map (Fig. 2) by taking the spectrally integrated transient absorption–time curves over the four distinctive wavelength windows from λ = 350–380, 440–520,

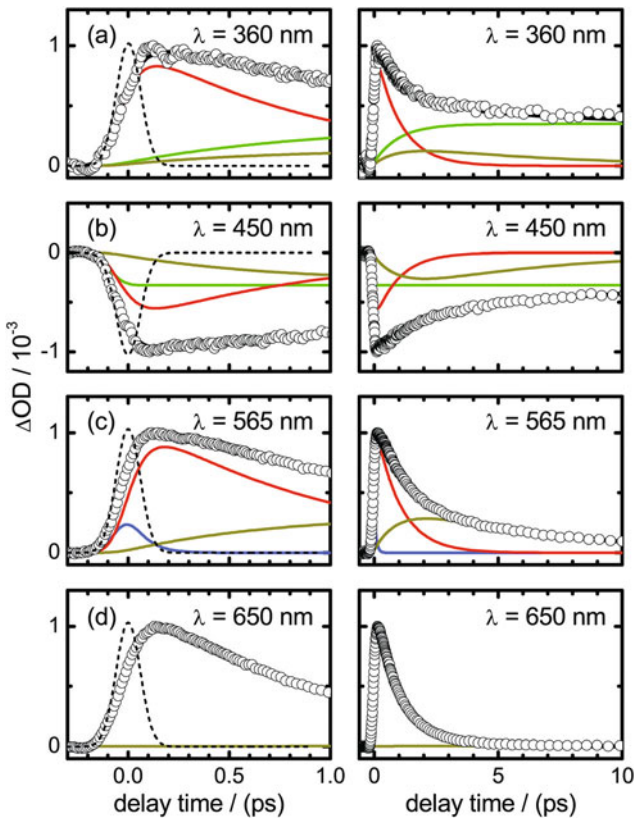

Fig. 4 Absorption–time profiles at four representative probe wavelengths (a–d) for delay times up to Δt = 1.0 ps (left column) and Δt = 10 ps (right column). Open circles are data, solid black lines the overall least-squares fit curves. The different contributions are indicated by coloured lines (blue: ESA_1; red: $ESA_{2,3}$; light brown: HGSA; green: permanent GSB resp. PA.) The thin dashed curves on the left show the IRF.

Table 1 Results of the global fit analysis of the absorption–time profiles of DR1 in 2FT. Values in parentheses give the 2σ standard deviations with respect to the last digits

λ/nm	τ_1/ps[a]	A_1 (rel.)	τ_2/ps	A_2 (rel.)	τ_3/ps	A_3 (rel.)	A_∞ (rel.)
360	0.076(2)	—	0.99(1)	0.82(3)	6.0(1)	0.12(3)	0.35(2)
450	0.076(2)	—	0.99(1)	−0.56(2)	6.0(1)	−0.26(2)	−0.32(2)
475	0.076(2)	—	0.99(1)	−0.63(1)	6.0(1)	−0.23(2)	−0.28(2)
560	0.076(2)	0.24(2)	0.99(1)	0.86(2)	6.0(1)	0.31(2)	—
565	0.076(2)	0.23(2)	0.99(1)	0.88(2)	6.0(1)	0.28(2)	—
570	0.076(2)	0.25(2)	0.99(1)	0.90(2)	6.0(1)	0.23(2)	—
575	0.076(2)	0.25(1)	0.99(1)	0.90(1)	6.0(1)	0.22(2)	—
580	0.076(2)	—	0.99(1)	0.94(2)	6.0(1)	0.18(2)	—
590	0.076(2)	—	0.99(1)	0.95(1)	6.0(1)	0.12(1)	—
600	0.076(2)	—	0.99(1)	0.95(1)	6.0(1)	0.07(2)	—
625	0.076(2)	—	0.99(1)	0.98(1)	6.0(1)	0.02(3)	—
650	0.076(2)	—	0.99(1)	0.99(1)	6.0(1)	0.01(3)	—

[a] The small statistical error limits arise because the values for τ_{IRF} and time-zero were kept fixed. Final results with error limits including estimated systematic uncertainties for τ_{IRF} and time-zero are given in the text.

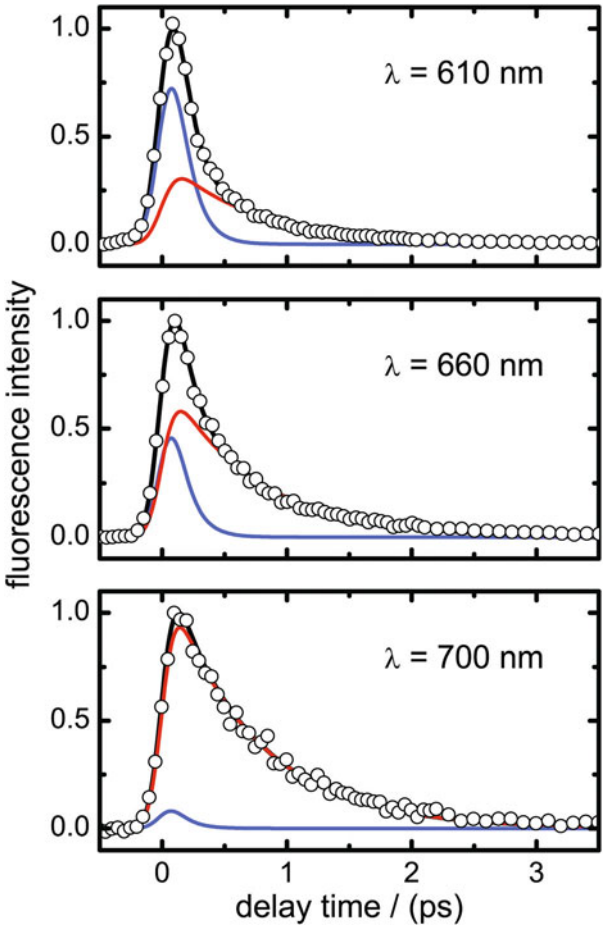

Fig. 5 Fluorescence–time profiles of DR1 in 2FT excited at λ_{pump} = 475 nm at three selected emission wavelengths. Open circles are data, solid black lines give the fitted curves, blue and red curves show the individual decay components.

545–575, and 580–650 nm. Only the 380–440 nm region was omitted, because the respective spectro-temporal contributions due to ESA decay, HGSA rise and HGSA decay, PA rise and GSB refill overlap too heavily in wavelengths and time in this range to allow for an unbiased fit without prohibitively large cross-correlations between the resulting parameters. Apart from this narrow range, however, this analysis covered the entire probe spectrum. The results for the time constants from this alternative approach were virtually identical with the ones determined above.

3.3. Time-resolved fluorescence measurements

Measured fluorescence decay curves at three selected emission wavelengths, λ_{fl} = 610, 660 and 700 nm, are shown in Fig. 5. The parameters which were extracted by least-squares fitting to the time profiles are collected in Table 2. As can be seen, all time profiles require two exponentials for modeling. However, the amplitude of the faster component decreases rapidly with longer emission wavelengths. At λ_{fl} = 600–610 nm, the fluorescence–time profile is almost completely determined by the fast first component, but only the longer-lived second component plays a role at λ_{fl} = 700 nm. Applying again a consecutive

Table 2 Results of the global fit analysis of the fluorescence–time profiles of DR1 in 2FT. Values in parentheses give the 2σ standard deviations with respect to the last digits

λ/nm	τ_1'/ps	A_1 (rel.)	τ_2'/ps	A_2 (rel.)
600	0.12(4)	0.74(5)	0.70(8)	0.26(2)
610	0.12(4)	0.71(8)	0.70(8)	0.29(2)
620	0.12(4)	0.63(4)	0.70(8)	0.37(2)
640	0.12(4)	0.47(9)	0.70(8)	0.53(2)
660	0.12(4)	0.43(7)	0.70(8)	0.57(3)
680	0.12(4)	0.30(9)	0.70(8)	0.70(6)
700	0.12(4)	0.08(9)	0.70(8)	0.92(6)

model, similar to above, the fitted fluorescence lifetimes (with 2σ statistical and estimated systematic error limits) of

$$\tau_1' = 0.12 \pm 0.06 \text{ ps},$$

$$\tau_2' = 0.70 \pm 0.10 \text{ ps}$$

correlate well with the excited-state lifetimes τ_1 and τ_2 determined by the transient absorption measurements.

4. Discussion

The time-resolved broadband absorption and fluorescence upconversion measurements presented above provide explicit information on the ultrafast photo-induced dynamics of the push–pull-substituted azobenzene Disperse Red 1. Special attention is directed at the very early dynamics, which has been analysed using a detailed kinetic model.

The obtained transient spectra clearly demonstrate a sequential temporal evolution of the molecules in the excited state within the first 300 fs after the pump pulse. The excited-state absorption in the λ_{probe} = 530–580 nm range (ESA_1) was found to rise earlier than the excited-state absorption at longer wavelengths (580–670 nm, ESA_2) or in the UV (350–415 nm, ESA_3). In the latter two regions, the band intensities reach their maxima with some delay, whereas the absorption in the first window has reached its peak in only ≈100–150 fs. Moreover, ESA_1 in the 530–580 nm range exhibits a very fast spectral blue-shift in the first ≈100–150 fs after the pump pulse, while ESA_2 from 580–670 nm continues to rise without a large spectral shift. Those different pieces of the puzzle add up to a picture that suggests an ultrafast transformation of the wavepacket prepared by the pump laser pulse from the ππ* optically excited (OE) state to an intermediate excited state (IE), or relaxed excited state (RE), at somewhat lower energy within $\Delta t \lesssim 100$ fs, before the excited molecules may return to the electronic ground state.

The global kinetic analysis of the absorption–time profiles gave quantitative insight into the related processes. The time-resolved experimental data could be nicely modeled assuming a sequential kinetic scheme, where the distinction between two "states" E^* and E^{**} and the proposition that E^{**} arises consecutively from E^* were made based on the transient spectra in Fig. 3a and on the earlier reports of a delayed ESA.[10,11] Accordingly, time constant τ_1 = 0.08 ± 0.03 ps is now assigned to the lifetime of the OE state with respect to its transition to the IE (or RE) state, while time constant τ_2 = 0.99 ± 0.02 ps gives the lifetime of the IE (or RE) state with respect to the *E*–*Z* isomerisation

and radiationless electronic conversion through the conical intersection (CI) connecting it with the S_0 electronic ground state. The resulting internally highly excited S_0 molecules thereafter undergo vibrational cooling described by time constant $\tau_3 = 6.0 \pm 0.1$ ps.

The results of the fluorescence up-conversion measurements, despite their lower temporal resolution, provide further support. The experimental data suggest that the fluorescence arises from two different types of excited states, where the energetically higher one decays faster and appears to populate the lower one by an ultrafast transformation. Most notable in this context is the rapidly decreasing amplitude of the faster fluorescence decay component (τ'_1) towards longer wavelengths. This translates into a fast red-shift of the emission spectrum as the wavepacket transforms from the OE to the IE/RE state, which fluoresces at longer wavelengths. The red-shift of the fluorescence correlates with the blue-shift in the excited-state absorption spectrum (ESA_1). On the other hand, the emission near the band maximum in the static spectrum ($\lambda_{fl} \approx 590$ nm, *cf*. Fig. 1) is highly predominated by the fast component. The fluorescence decay times $\tau'_1 = 0.12 \pm 0.06$ ps and $\tau'_2 = 0.70 \pm 0.10$ ps correspond well in magnitude to τ_1 and τ_2 from the absorption measurement. The deviations can be rationalised by differences between the FC windows for the $S_2/S_1 \rightarrow S_0$ transition seen in fluorescence and the $S_n/S_m \leftarrow S_2/S_1$ transitions probed in absorption. Considering the sub-picosecond fluorescence lifetime, we note without going into more detail that it is highly unlikely that solvent relaxation around the excited-state molecules is complete. The observable Stokes shift ($\Delta\lambda \approx 115$ nm) in the static fluorescence spectrum therefore very likely does not reflect the solvent stabilisation of a fully relaxed excited state.

Bi- or multiphasic fluorescence dynamics similar to the experimentally observed behaviour can, in principle, arise from several different mechanisms. The first is vibrational relaxation in the excited state. In view of the well-known much longer time scale (≈10 ps) for typical vibrational energy transfer processes to an organic solvent compared to our τ_1 (≈80 fs), this possibility can be ruled out. The second possibility is a dynamic Stokes shift due to solvation dynamics around the solute molecules after the photoexcitation. Solvent relaxation is known to be multiphasic, with an ultrafast (1 ps) component arising from inertial reorientation of the solvent molecules and longer-lived components associated with slower diffusional motion.[45,46] Both contributions are revealed by corresponding dynamic Stokes shifts in the associated transient fluorescence spectra. In general, it is possible to reconstruct the transient fluorescence spectra from the measured fluorescence–time profiles at a range of emission wavelengths. In our case, however, an intense solvent Raman signal prevented us from recording any fluorescence–time profiles at wavelengths around the maximum of the static fluorescence spectrum at $\lambda_{fl} \approx 590$ nm (*cf*. Fig. 1) and below so that it was not possible to recover the complete transient spectra for DR1. The long-wavelength wings of the transient spectra, which we could reconstruct, do show a time-dependent red-shift as could be expected from the fluorescence–time profiles. However, several arguments speak against an explanation of this red-shift by solvation dynamics.

First, all fluorescence–time profiles could be well described with only two distinctive decay times, τ'_1 and τ'_2, over the entire wavelength range. Typical solvation processes show an initial decay at the blue side, a rise at the red side of the fluorescence spectrum, and a wavelength-dependent continuous change of the time constants in between (see, *e.g.*, ref. 47). While the rise on the red may have been obscured due to the fast fluorescence decay, we clearly did not observe a continuous evolution of the time constants. Second, known typical solvent reorientation times (with the exception of the special case of water[48]) are usually somewhat longer than ≈1 ps,[45,47,49] especially considering relatively large molecules such as 2FT, in contrast with our sub-100 fs value of τ_1. Third, the apparent spectral shifts in the recorded 2D absorption map for DR1 are localized to a rather narrow spectral window. Hence, although some contributions by solvent relaxation cannot be excluded, solvation dynamics does not seem to be the major cause for the observed spectral changes.

The third explanation for the biphasic dynamics is an ultrafast radiationless electronic transition. A sequential transformation from the optically excited state *via* an intermediate state to the ground state in push–pull azobenzenes has been presumed in previous studies.[10,11,35] However, the prompt, IRF-limited appearance of the ESA_1 band after the excitation laser pulse has not been fully recognized and taken into account before, probably because of its relatively narrow spectral width, and because its subsequent decay is partially masked by the rising ESA_2 band ($\Delta t < 300$ fs) and the HGSA at longer times ($\Delta t > 1$ ps). Schmidt *et al*., who reported time-resolved emission and absorption measurements on DMANAB in toluene,[10] observed a biphasic fluorescence decay with a short first lifetime of $\tau_1 \approx 100$ fs and a delayed ESA rise, but based on a comparison with plain AB they associated τ_1 with a rapid departure of the excited wavepacket from the FC region of the photo-excited state instead of a fast internal conversion between two excited states. Poprawa-Smoluch *et al.* studied the ultrafast kinetics and anisotropy of DR1 in toluene, acetonitrile and ethylene glycol,[11] but could not fully resolve the very early events at the time. In spite of this, they also report a delayed ESA appearance at $\lambda > 600$ nm with a rise time of $\tau_1 < 200$ fs, which they assigned to rapid internal conversion of the initially excited ππ* state to the energetically lower nπ* state. Meanwhile, Hsu *et al*.[35] interpreted their results similar to Schmidt *et al.* The slower second time constant, $\tau_2 \approx 1$ ps, has been commonly accepted as the lifetime of the excited molecules with respect to the isomerisation and radiationless deactivation to the S_0 state.

The kinetic model applied to the experimental data in the present work accounts for the observed photochemical dynamics of DR1 overall in a global fashion. However, the energetic order of the excited states of DR1 and the nature of the intermediate excited state remain under question. For the case of 4-methoxy-4′-nitro-azobenzene (MNAB), the ππ* state is supposed to be clearly higher (S_2) in energy at vertical excitation than the nπ* state (S_1).[9] For 4-dimethylamino-4′-nitro-azobenzene (DMANAB) and DR1, the energetic order is less certain and depends on the solvent. Quantum chemical calculations employing basis sets of double-zeta quality indicated that the nπ* state is slightly lower than the first ππ* state,[11,38,39] but larger basis sets would be needed for more conclusive evidence. Based on a spectral decomposition study of the fluorescence spectra, the two states are supposed to keep their order even in

highly polar solvents like acetonitrile, but rearrange in alcohols, where the ππ* state thus falls below the nπ* state.[36,37] The rapid internal conversion from the optically bright ππ* state to the nπ* state prior to the return to the S_0 state proposed by Poprawa-Smoluch *et al.* implicitly assumes an energetically higher ππ* state. On the other hand, the peak absorption wavelength of λ_{max} = 475 nm of the strong ππ* transition of DR1 corresponds to lower energy than the known absorption maximum at λ_{max} = 450 nm of the nπ* band of plain AB. The situation might be even more complex, however. A resonance Raman study on DMANAB led Biswas and Umpathy to conclude that the solvent environment strongly influences the ππ* excited state. They distinguished between the ππ*/OE state reached in *n*-hexane and the solvent-stabilised "relaxed" ππ*/CT state that is reached in <100 fs from the ππ*/OE state in benzene.[32,33] This relaxation is due to an adiabatic change in the electronic structure of the OE/CT state with solvent polarity, rather than a complete change of the electronic character.

In view of the uncertainty about the energetic order of the ππ* and nπ* states, we propose two alternative scenarios for the photo-induced dynamics of DR1 after excitation at λ_{pump} = 475 nm as depicted in Fig. 6. In the first scenario (Fig. 6a), the pump laser pulse projects a wavepacket from S_0 to the FC region of the optically bright ππ* state, which is observable for roughly ≈100 fs in emission around 600 nm and in transient absorption around $\lambda \approx 570$ nm (ESA_1). Very rapid internal conversion, however, takes the wavepacket from the ππ* (OE) state in 100 fs (τ_1) to the energetically lower nπ* (IE) state. The nπ* state is well detected by several intense excited-state absorptions (ESA_2, ESA_3). The observation of the weaker longer-lived fluorescence component suggests that the two excited states are vibronically quite strongly coupled. The subsequent isomerisation and radiationless deactivation to the electronic ground state takes place in ≈1.0 ps (τ_2). The reaction coordinate to the nπ*/S_0 CI likely involves torsional motion around the central CNNC coordinate as in plain AB.

In the second scenario (Fig. 6b), the ππ* (OE) state may be below the nπ* (IE) state at vertical excitation. Without an easily accessible ππ*/S_0 CI, however, the relaxation to the S_0 state can occur only *via* the nπ* state, which is reached *via* a rapid internal conversion in the time of τ_1 from the ππ* state at some configuration, where nπ* moves below ππ*. The isomerisation and deactivation to S_0 in time τ_2 thus takes place again along the CNNC torsional coordinate *via* the nπ*/S_0 CI.

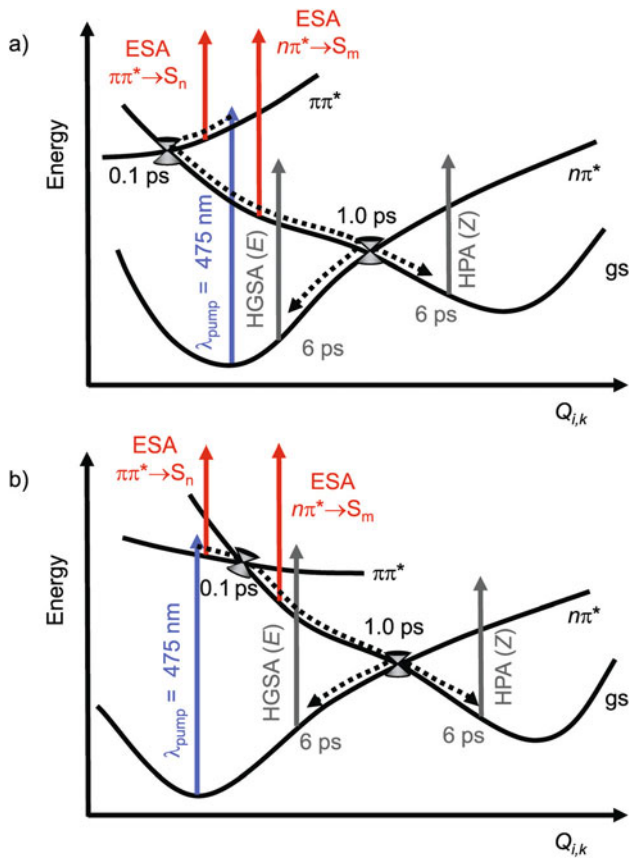

Fig. 6 Proposed relaxation pathways for DR1 after photoexcitation at λ_{pump} = 475 nm. (a) The ππ* state is above the nπ* state at vertical excitation and the deactivation to the S_0 state occurs stepwise by internal conversion to the lower-lying nπ* state and the CI between the nπ* and S_0 states involving the CNNC torsional pathway as in plain AB. (b) The ππ* state is below the nπ* state at vertical excitation, but the deactivation to the S_0 state occurs sequentially by rapid motion of the wavepacket from the ππ* to the nπ* state and the nπ*/S_0 CI along the CNNC torsional coordinate.

5. Conclusion

In conclusion, we have presented a study of the photo-induced dynamics of the push–pull azobenzene Disperse Red 1 in solution in 2-fluorotoluene by means of femtosecond time-resolved transient absorption spectroscopy and fluorescence up-conversion spectroscopy following photoexcitation at λ_{pump} = 475 nm. The observed transient excited-state absorption spectra in the first ≈300 fs after the pump laser pulse, the experimental absorption–time profiles, and the observed biphasic fluorescence decay dynamics demonstrate a stepwise electronic deactivation and isomerisation. A consecutive kinetic model allowed for a global analysis of the transient absorption–time profiles with three time constants, τ_1 = 80 ± 30 fs, τ_2 = 0.99 ± 0.02 ps and τ_3 = 6.0 ± 0.1 ps, which account for the present experimental results and for previously reported data in the literature. Therefore, τ_1 was assigned to the internal conversion and relaxation of the initially excited ππ* state to the nπ* state, τ_2 to the radiationless transformation from the nπ* to the ground electronic state and the *E–Z* isomerisation and τ_3 to the eventual vibrational cooling processes in the electronic ground state. The question of the energetic ordering of the ππ* and nπ* states at vertical excitation remains undecided, both states are clearly very close in energy.

Last but not least, this study of the azo dye DR1 in solution provides a basis for the interpretation of new experiments on the photodynamics of DR1 in complex environments and photoswitchable materials under application-relevant conditions, *e.g.*, in polymeric organic films or glasses. Towards these ends, a time-resolved fluorescence study of the photoisomerisation of DR1 in a polybutylmethacrylate matrix has just been completed in our laboratory to obtain insight into the effects of the topographic constraints by the polymeric micronetwork on the ensuing reaction dynamics.[20]

Acknowledgements

This work has been supported by the Deutsche Forschungsgemeinschaft through project A1 of the Sonderforschungsbereich 677 "Function by Switching".

References

1 Z. F. Liu, K. Hashimoto and A. Fujishima, Photoelectrochemical information storage using an azobenzene derivative, *Nature*, 1990, **347**, 658–660.
2 T. Ikeda and O. Tsutsumi, Optical switching and image storage by means of azobenzene liquid-crystal films, *Science*, 1995, **268**, 1873–1875.
3 I. Willner and S. Rubin, Control of the structure and functions of biomaterials by light, *Angew. Chem., Int. Ed. Engl.*, 1996, **35**, 367–385.
4 H. Rau, Azo compounds, in *Photochromism: Molecules and Systems*, ed. H. Dürr and H. Bouas-Laurent, Elsevier, Amsterdam, 2003.
5 V. Balzani, A. Credi and M. Venturi, *Molecular Devices and Machines: Concepts and Perspectives for the Nanoworld*, Wiley-VCH, Weinheim, 2nd edn, 2008.
6 *Molecular Switches*, ed. B. L. Feringa and W. R. Brown, Wiley-VCH, Weinheim, 2011, vol. 1 & 2.
7 J. A. Delaire and K. Nakatani, Linear and nonlinear optical properties of photochromic molecules and materials, *Chem. Rev.*, 2000, **100**, 1817–1845.
8 H. M. D. Bandara and S. C. Burdette, Photoisomerization in different classes of azobenzene, *Chem. Soc. Rev.*, 2012, **41**, 1809–1825.
9 M. Hagiri, N. Ichinose, C. Zhao, H. Horiuchi, H. Hiratsuka and T. Nakayama, Sub-picosecond time-resolved absorption spectroscopy of a *push–pull* type *p,p′*-substituted *trans*-azobenzene, *Chem. Phys. Lett.*, 2004, **391**, 297–301.
10 B. Schmidt, C. Sobotta, S. Malkmus, S. Laimgruber, M. Braun, W. Zinth and P. Gilch, Femtosecond fluorescence and absorption dynamics of an azobenzene with a strong push–pull substitution, *J. Phys. Chem. A*, 2004, **108**, 4399–4404.
11 M. Poprawa-Smoluch, J. Baggerman, H. Zhang, H. P. A. Maas, L. De Cola and A. M. Brouwer, Photoisomerization of Disperse Red 1 studied with transient absorption spectroscopy and quantum chemical calculations, *J. Phys. Chem. A*, 2006, **110**, 11926–11937.
12 T. Asano, Pressure effects on the thermal *cis–trans* isomerization of 4-dimethylamino-4′-nitroazobenzene. Evidence for a change of mechanism with solvent, *J. Am. Chem. Soc.*, 1980, **102**, 1205–1206.
13 K. Gille, H. Knoll and K. Quitzsch, Rate constants for the thermal *cis–trans* isomerization of azobenzene dyes in solvents, acetone–water mixtures and in microheterogeneous surfactant solutions, *Int. J. Chem. Kinet.*, 1999, **31**, 337–350.
14 A. Natansohn and P. Rochon, Photoinduced motions in azo-containing polymers, *Chem. Rev.*, 2002, **102**, 4139–4175.
15 P. Rochon, E. Batalla and A. Natansohn, Optically induced surface gratings on azoaromatic polymer films, *Appl. Phys. Lett.*, 1995, **66**, 136–138.
16 S. Yokoyama, T. Nakahama, A. Otomo and S. Mashiko, Intermolecular coupling enhancement of the molecular hyperpolarizability in multichromophoric dipolar dendrons, *J. Am. Chem. Soc.*, 2000, **122**, 3174–3181.
17 J. Martinez-Perdiguero, Y. Zhang, C. Walker, J. Etxebarria, C. L. Folcia, J. Ortega, M. J. O'Callaghan and U. Baumeister, Second harmonic generation in laterally azo-bridged H-shaped ferroelectric dimesogens, *J. Mater. Chem.*, 2010, **20**, 4905–4909.
18 D. Marinotto, S. Proutière, C. Dragonetti, A. Colombo, P. Ferruti, D. Pedron, M. Ubaldi and S. Pietralunga, Evidence for the applicability of a novel procedure (swelling–poling–deswelling) to produce a stable alignment of second order NLO-chromophores covalently attached to a cross-linked PMMA or polystyrene polymeric network, *J. Non-Cryst. Solids*, 2011, **375**, 2075–2080.
19 M. E. El-Khouly, Y. Chen, X. Zhuang and S. Fukuzumi, Long-lived charge-separated configuration of a push-pull archetype of Disperse Red 1 end-capped poly[9,9-bis(4-diphenylaminophenyl)fluorene], *J. Am. Chem. Soc.*, 2009, **131**, 6370–6371.
20 J. Bahrenburg, F. Renth, F. Plamper, T. Eckert, W. Richtering and F. Temps, Huge differences between the ultrafast photoisomerization dynamics of azobenzenes in polymers and in solution, submitted.
21 H. Satzger, S. Spörlein, C. Root, J. Wachtveitl, W. Zinth and P. Gilch, Fluorescence spectra of *trans*- and *cis*-azobenzene – emission from the Franck–Condon state, *Chem. Phys. Lett.*, 2003, **372**, 216–223.
22 C.-W. Chang, Y.-C. Lu, T.-T. Wang and E. W.-G. Diau, Photoisomerization dynamics of azobenzene in solution with S_1 excitation: a femtosecond fluorescence anisotropy study, *J. Am. Chem. Soc.*, 2004, **126**, 10109–10118.
23 T. Pancur, F. Renth, F. Temps, B. Harbaum, A. Krüger, R. Herges and C. Näther, Femtosecond fluorescence up-conversion spectroscopy of a rotation-restricted azobenzene after excitation to the S_1 state, *Phys. Chem. Chem. Phys.*, 2005, **7**, 1985–1989.
24 R. Siewertsen, J. B. Schönborn, B. Hartke, F. Renth and F. Temps, Superior $Z \rightarrow E$ and $E \rightarrow Z$ photoswitching dynamics of dihydrodibenzodiazocine, a bridged azobenzene, by $S_1(n\pi^*)$ excitation at λ = 387 and 490 nm, *Phys. Chem. Chem. Phys.*, 2011, **13**, 1054–1063.
25 P. Cattaneo and M. Persico, An *ab initio* study of the photochemistry of azobenzene, *Phys. Chem. Chem. Phys.*, 1999, **1**, 4739–4743.
26 C. Ciminelli, G. Granucci and M. Persico, Are azobenzenophanes rotation-restricted?, *J. Chem. Phys.*, 2005, **123**, 174317.
27 C. Nonnenberg, H. Gaub and I. Frank, First-principles simulation of the photoreaction of a capped azobenzene: the rotational pathway is feasible, *ChemPhysChem*, 2006, **7**, 1455–1461.
28 G. Granucci and M. Persico, Excited state dynamics with the direct trajectory surface hopping method: azobenzene and its derivatives as a case study, *Theor. Chem. Acc.*, 2007, **117**, 1131–1143.
29 I. Conti, M. Garavelli and G. Orlandi, The different photoisomerization efficiency of azobenzene in the lowest $n\pi^*$ and $\pi\pi^*$ singlets: the role of a phantom state, *J. Am. Chem. Soc.*, 2008, **130**, 5216–5230.
30 O. Carstensen, J. Sielk, J. B. Schönborn, G. Granucci and B. Hartke, Unusual photochemical dynamics of a bridged azobenzene derivative, *J. Chem. Phys.*, 2010, **133**, 124305.
31 M. Pederzoli, J. Pittner, M. Barbatti and H. Lischka, Nonadiabatic molecular dynamics study of the *cis–trans* photoisomerization of azobenzene excited to the S_1 state, *J. Phys. Chem. A*, 2011, **115**, 11136–11143.
32 N. Biswas and S. Umapathy, Study of solvent effects on the molecular structure and the reorganization energies of 4-nitro-4′-dimethylaminoazobenzene using resonance Raman intensities, *J. Raman Spectrosc.*, 2001, **32**, 471–480.
33 N. Biswas and S. Umapathy, Resonance Raman study of the solvent dynamics for ultrafast charge transfer transition in 4-nitro 4′-dimethylamino-azobenzene, *J. Chem. Phys.*, 2003, **118**, 5526–5536.
34 F. O. Koller, C. Sobotta, T. E. Schrader, T. Cordes, W. J. Schreier, A. Sieg and P. Gilch, Slower processes of the ultrafast photo-isomerization of an azobenzene observed by IR spectroscopy, *Chem. Phys.*, 2007, **341**, 258–266.
35 C.-C. Hsu, Y.-T. Wang, A. Yabushita, C.-W. Luo, Y.-N. Hsiao, S.-H. Lin and T. Kobayashi, Environment-dependent ultrafast photoisomerization dynamics in azo dye, *J. Phys. Chem. A*, 2011, **115**, 11508–11514.
36 C. Toro, A. Thibert, L. De Boni, A. E. Masunov and F. E. Hernandez, Fluorescence emission of disperse red 1 in solution at room temperature, *J. Phys. Chem. B*, 2008, **112**, 929–937.
37 L. De Boni, C. Toro, A. E. Masunov and F. E. Hernandez, Untangling the excited states of DR1 in solution: an experimental and theoretical study, *J. Phys. Chem. A*, 2008, **112**, 3886–3890.
38 C. R. Crecca and A. E. Roitberg, Theoretical study of the isomerization mechanism of azobenzene and disubstituted azobenzene derivatives, *J. Phys. Chem. A*, 2006, **110**, 8188–8203.
39 L. X. Wang and X. G. Wang, *Ab initio* study of photoisomerization mechanisms of *push–pull p,p′*-disubstituted azobenzene derivatives on S_1 excited state, *THEOCHEM*, 2007, **847**, 1–9.
40 F. Renth, M. Foca, A. Petter and F. Temps, Ultrafast transient absorption spectroscopy of the photoinduced *Z–E* isomerization of a photochromic furylfulgide, *Chem. Phys. Lett.*, 2006, **428**, 62–67.
41 R. Siewertsen, F. Renth and F. Temps, Parallel ultrafast *E–C* ring closure and *E–Z* isomerisation in a photochromic furylfulgide studied by femtosecond time-resolved spectroscopy, *Phys. Chem. Chem. Phys.*, 2009, **11**, 5952–5961.
42 T. Pancur, N. K. Schwalb, F. Renth and F. Temps, Femtosecond fluorescence up-conversion spectroscopy of adenine and adenosine: experimental evidence for the $\pi\sigma^*$ state?, *Chem. Phys.*, 2005, **313**, 199–212.
43 N. K. Schwalb and F. Temps, A modified four-state model for the "dual fluorescence" of N^6,N^6-dimethyladenine derived from femtosecond fluorescence spectroscopy, *J. Phys. Chem. A*, 2009, **113**, 13113–13123.
44 C. Wohlfahrt, Static dielectric constants of pure liquids and binary liquid mixtures, in *Springer Materials – the Landolt–Börnstein Database*, ed. O. Madelung, Springer, Berlin, 1991, vol. 6, pp. 5–228.
45 M. Maroncelli, J. MacInnis and G. R. Fleming, Polar solvent dynamics and electron-transfer reactions, *Science*, 1989, **243**, 1674–1681.

46 M. Maroncelli and G. R. Fleming, Picosecond solvation dynamics of coumarin 153: the importance of molecular aspects of solvation, *J. Chem. Phys.*, 1987, **86**, 6221–6239.
47 D. Zhong, S. Kumar Pal, D. Zhang, S. I. Chan and A. H. Zewail, Femtosecond dynamics of rubredoxin: tryptophan solvation and resonance energy transfer in the protein, *Proc. Natl. Acad. Sci. U. S. A.*, 2002, **99**, 13–18.
48 S. K. Pal, J. Peon, B. Bagchi and A. H. Zewail, Biological water: femtosecond dynamics of macromolecular hydration, *J. Phys. Chem. B*, 2002, **106**, 12376–12395.
49 M. C. Stuhldreier, M. Malicki, H. Böhnke, N. Öksüz, J. Keppler, K. Schwarz and F. Temps, Ultrafast solvation dynamics of ferulic acid in a micellar environment, to be published.